

Lattice and elastic constants of titanium-niobium monoborides containing aluminum and vanadium

D. R. Trinkle*

Materials and Manufacturing Directorate, Air Force Research Laboratory,
Wright Patterson Air Force Base, Dayton, Ohio 45433-7817

(Dated: December 22, 2021)

First-principles electronic-structure computes the lattice and elastic constants of single-crystal TiB and NbB and changes with Nb, Ti, Al, and V solutes. The data is built into an interpolation formula for lattice and elastic constants of the quaternary (TiNbAlV)B with dilute Al and V concentrations. The lattice and elastic constants of borides in two Ti alloys containing Nb and Al are predicted from microprobe measurements.

Keywords: Elastic behavior; Titanium alloys; Transition metals; Borides; Density functional

Introduction. Strengthening titanium alloys with titanium-monoboride (TiB) combines the beneficial stiffness properties of TiB with the plastic behavior of a titanium alloy matrix, increasing the range of applicability for automotive and aerospace applications. The Ti-TiB composites have increased stiffness, high-temperature strength, creep performance, fatigue and wear resistance[1, 2, 3]. Borides also influence the morphology of α phase in α/β Ti alloys, producing microstructures similar to recrystallized alloys[4]. Despite the importance of TiB, accurate predictions of titanium-monoboride elastic constants have only happened recently[5]. Titanium-boride has the FeB structure: a primitive orthorhombic structure with space group $Pnma$ [6]. The lattice constants measured with x-ray powder diffraction are $a_0 = 6.12 \pm 0.01 \text{ \AA}$, $b_0 = 3.06 \pm 0.01 \text{ \AA}$, and $c_0 = 4.56 \pm 0.01 \text{ \AA}$ [7]. The eight-atom unit cell has four equivalent Ti atoms at the c Wyckoff positions (0.177, 0.25, 0.123) and four equivalent B atoms at the c Wyckoff position (0.029, 0.25, 0.603). Direct measurements of the 9 independent single-crystal elastic constants are difficult, and instead elastic-constant combinations have previously been inferred from Ti-TiB composite measurements[8, 9]. Panda and Chandran have filled the gap of experimental measurements with density-functional calculations of the elastic constants of pure TiB[5].

In order to make accurate predictions about the lattice and elastic constants of monoboride inclusions in titanium alloys, it is necessary to include the effects of off-stoichiometric chemistries sampled in the monoborides. These titanium alloys often include aluminum, vanadium, and niobium additions. While the borides formed in these alloys are expected to remain near 50 at.% B composition, potentially any of the four metals may occupy the metallic sublattice. Microprobe measurements of borides in titanium alloys containing niobium have found a nearly equal concentration of Ti and Nb in the borides[10]. Metallographic investigation of alloys in the Ti-V-B system has found comparable V concentration in the metal matrix and borides after partitioning[11]. Given the difficulty of elastic property measurements for the small dispersed borides, density-functional theory can be used to predict the missing data. Here, a predictive model of lattice and elastic constants for (TiNbAlV)B in the dilute Al and V limit is constructed using density-functional theory calculations of

TiB and NbB properties, combined with misfits due to Nb, Ti, Al, and V solutes, all at zero temperature. The predictions of the model are compared with a quasirandom (TiNb)B alloys to demonstrate the accuracy of the interpolation. Finally, the lattice and elastic constants are predicted for borides using compositions taken from microprobe measurements in actual alloys[10].

Methods. The *ab initio* calculations are performed with VASP [12, 13], a density-functional code using a plane-wave basis and the projector augmented-wave (PAW) method[14], with potentials generated by Kresse[15]. The generalized-gradient approximation of Perdew and Wang is employed[16]. In order to ensure accurate treatment of the boron potential, a plane-wave kinetic-energy cutoff of 319 eV is used. The k -point meshes for the 8-atom pure monoboride cells are $7 \times 14 \times 10$ and $7 \times 5 \times 5$ for the 48-atom $1 \times 3 \times 2$ supercells, with a Methfessel-Paxton smearing of 0.2 eV. The PAW potentials for boron and aluminum treat the s and p states as valence, while the titanium, vanadium, and niobium potentials treat the s , d , and filled- p states as valence, corresponding to a core atomic reference configurations of He for B, Ne for Al, Mg for Ti and V, and Ca for Nb. In all cases, the internal atomic forces are relaxed to less than 5 meV/ \AA , and the stresses are relaxed to less than 0.2 kbar to determine lattice constants.

The changes in lattice and elastic constants of TiB and NbB with dilute substitutions of Nb, Ti, Al, and V are extracted from a systematic series of relaxed and strained supercells, all at 0K. First, the TiB, NbB, and (48-atom) quasirandom (Ti_{0.75}Nb_{0.25})B, (Ti_{0.5}Nb_{0.5})B, and (Ti_{0.25}Nb_{0.75})B lattice constants are determined via conjugate-gradient minimization. Special quasirandom structures[17, 18] are periodic supercells where the chemical species are chosen to most closely approximate a random structure; c.f., Figure 1. The quasirandom structures were constructed using the program ATAT [19]. To determine the elastic constants, relaxed cells are subjected to different magnitudes of one volumetric strain and six volume-conserving strains (c.f., Table I); the magnitudes range from $\delta = -0.005$ to $\delta = +0.005$ in steps of 0.001. After the atomic degrees of freedom in each strained cell are fully relaxed, the stresses are calculated. Each stress σ_i is a linear combination of strains e_j and elastic constants C_{ij} : $\sigma_i = \sum_j C_{ij}e_j$; c.f., Table I. The ratio of stress to δ from positive and negative δ values are averaged. A range of strains is used to check that

TABLE I: One volumetric and six volume-conserving strain combinations and the linearized stress responses used to compute elastic constants in monoborides. The magnitude of each strain is given by a single parameter δ that can be positive or negative. The linear response of stress to strain is determined by a linear combination of elastic constants, and these linear combinations are inverted to determine the elastic constants from the electronic-structure calculations. The first strain combination is a purely volumetric strain; the remaining six combinations conserve volume for all δ . The first four strain combinations produce stresses dependent on C_{11} , C_{22} , C_{33} , C_{12} , C_{23} , and C_{13} ; the final three give C_{44} , C_{55} , and C_{66} .

$\underline{e_1}$	$\underline{e_2}$	$\underline{e_3}$	$\underline{\sigma_1/\delta}$	$\underline{\sigma_2/\delta}$	$\underline{\sigma_3/\delta}$
δ	δ	δ	$C_{11} + C_{12} + C_{13}$	$C_{22} + C_{12} + C_{23}$	$C_{33} + C_{23} + C_{13}$
δ	$-\delta$	$\frac{\delta^2}{1-\delta^2}$	$C_{11} - C_{12}$	$-C_{22} + C_{12}$	$-C_{23} + C_{13}$
$\frac{\delta^2}{1-\delta^2}$	δ	$-\delta$	$C_{12} - C_{13}$	$C_{22} - C_{23}$	$-C_{33} + C_{23}$
$-\delta$	$\frac{\delta^2}{1-\delta^2}$	δ	$-C_{11} + C_{13}$	$-C_{12} + C_{23}$	$C_{33} - C_{13}$
<hr/>					
$e_4 = \delta$,	$e_1 = \frac{\delta^2}{4-\delta^2}$			$\sigma_4/\delta = C_{44}$	
$e_5 = \delta$,	$e_2 = \frac{\delta^2}{4-\delta^2}$			$\sigma_5/\delta = C_{55}$	
$e_6 = \delta$,	$e_3 = \frac{\delta^2}{4-\delta^2}$			$\sigma_6/\delta = C_{66}$	

the effect of anharmonicity is negligible; the elastic constant combinations change by less than 0.1% between $\delta = 0.005$ and $\delta = 0.001$. The values for C_{44} , C_{55} , and C_{66} are extracted directly from corresponding strains; the other six elastic constants C_{11} , C_{22} , C_{33} , C_{12} , C_{23} , and C_{13} are extracted from a least-squares fit of the 12 data from the first four strains in Table I. To compute lattice and elastic misfits, $1 \times 3 \times 2$ supercells of 24 metal ions and 24 boron ions are constructed; a single Al, V, Ti or Nb ion is substituted for one metal ion in the cell. Each 48-atom cell is relaxed to extract lattice constants; the cells break orthorhombic symmetry slightly, producing monoclinic strains of less than 10^{-3} . These monoclinic strains are removed before calculation of elastic constants, which proceeds in an identical manner to the TiB and NbB cases, using $\delta = \pm 0.005$ for the volumetric strains, and $\delta = \pm 0.004$ and ± 0.002 for the volume-conserving strains. The misfit for lattice or elastic constant y of each metal species $X=\text{Al, V, and Nb}$ is numerically extracted as

$$\frac{1}{y} \frac{dy(\text{TiB})}{dc_X} = 24 \cdot \ln \left\{ \frac{y(X_{1/24}\text{Ti}_{23/24}\text{B}_{24})}{y(\text{TiB})} \right\} \quad (1)$$

for TiB, and similarly for NbB with $X=\text{Al, V, and Ti}$.

The composition of a general monoboride $(\text{TiNbAlV})\text{B}$ is given in terms of the atomic compositions of the four metal elements, c_{Ti} , c_{Nb} , c_{Al} , and c_{V} , under the assumption that metal ions only occupy the metal sublattice, and boron ions the boron sublattice. The alloy concentration is parameterized in the dilute Al and V limit, assuming a random metal sublattice,

TABLE II: Lattice and elastic misfits for Al and V substitutions in TiB and NbB. The misfit for a lattice or elastic constant y for solute X is defined as $y^{-1}dy/dc_X(c_X = 0)$. The values are extracted from 48 atom monoboride supercells, corresponding to an impurity concentration of 4.2 at.% The overall effect of Al and V additions is a volume shrinkage for TiB and NbB. Al weakens the elastic response of TiB and NbB, while V strengthens the elastic response of TiB and weakens NbB.

	TiB		NbB	
	Al	V	Al	V
$a^{-1}da/dc_X$	-0.0004	-0.0549	+0.0502	-0.0351
$b^{-1}db/dc_X$	-0.0155	-0.0238	-0.1305	-0.0426
$c^{-1}dc/dc_X$	-0.0262	-0.0370	+0.0378	-0.0351
$C_{11}^{-1}dC_{11}/dc_X$	-0.5087	+0.1292	-1.0050	-0.2961
$C_{22}^{-1}dC_{22}/dc_X$	-0.5067	+0.0513	-0.7241	-0.2352
$C_{33}^{-1}dC_{33}/dc_X$	-0.9164	+0.2021	-1.3733	-0.0992
$C_{12}^{-1}dC_{12}/dc_X$	-0.7691	-0.0390	-0.1827	+0.0932
$C_{23}^{-1}dC_{23}/dc_X$	+1.5049	+0.5071	+0.7557	-0.0166
$C_{13}^{-1}dC_{13}/dc_X$	+0.3567	+0.2501	-0.5439	-0.6332
$C_{44}^{-1}dC_{44}/dc_X$	-0.6064	+0.2187	-0.2334	+0.0255
$C_{55}^{-1}dC_{55}/dc_X$	-1.3375	-0.0543	-1.8392	-0.4602
$C_{66}^{-1}dC_{66}/dc_X$	-0.9031	+0.3123	-1.2579	-0.2825

tice, with equal partitioning of Al and V to Ti and Nb sites,

$$\begin{aligned} & [\text{Ti}_{(1-x)(1-(\alpha+\beta))}\text{Nb}_{x(1-(\alpha+\beta))}\text{Al}_{\alpha}\text{V}_{\beta}]\text{B} : \\ & x = \frac{c_{\text{Nb}}}{c_{\text{Ti}} + c_{\text{Nb}}} = 1 - \frac{c_{\text{Ti}}}{c_{\text{Ti}} + c_{\text{Nb}}}; \\ & \alpha = \frac{c_{\text{Al}}}{c_{\text{Ti}} + c_{\text{Nb}} + c_{\text{Al}} + c_{\text{V}}}; \quad \beta = \frac{c_{\text{V}}}{c_{\text{Ti}} + c_{\text{Nb}} + c_{\text{Al}} + c_{\text{V}}}, \quad (2) \end{aligned}$$

where x is the relative addition of Nb to Ti, and α and β are the additions of Al and V, respectively. The dilute Al and V limit corresponds to $\alpha \ll 1$ and $\beta \ll 1$. Lattice and elastic constants for a given monoboride alloy concentration are interpolated from the limiting TiB and NbB values using the cubic polynomial in x ,

$$\begin{aligned} y(x, \alpha, \beta) = & (1 - 3x^2 + 2x^3) \left[y(\text{TiB}) + \alpha \frac{dy(\text{TiB})}{dc_{\text{Al}}} + \beta \frac{dy(\text{TiB})}{dc_{\text{V}}} \right] \\ & + (3x^2 - 2x^3) \left[y(\text{NbB}) + \alpha \frac{dy(\text{NbB})}{dc_{\text{Al}}} + \beta \frac{dy(\text{NbB})}{dc_{\text{V}}} \right] \\ & + x(1-x)^2 \frac{dy(\text{TiB})}{dc_{\text{Nb}}} + (1-x)x^2 \frac{dy(\text{NbB})}{dc_{\text{Ti}}}, \quad (3) \end{aligned}$$

where y represents the given lattice or elastic constant, and all derivatives are evaluated in the dilute concentration limit from Eqn. (1). The interpolation formula builds the quaternary random alloy response from the six dilute binary alloy responses. It assumes that the misfits sum linearly, and interpolates properties of $(\text{Ti}_{1-x}\text{Nb}_x)\text{B}$ as a cubic polynomial in x .

Results. Figure 2 and Figure 3 show the lattice and elastic constants for the random $(\text{Ti}_{1-x}\text{Nb}_x)\text{B}$ alloy as interpolated

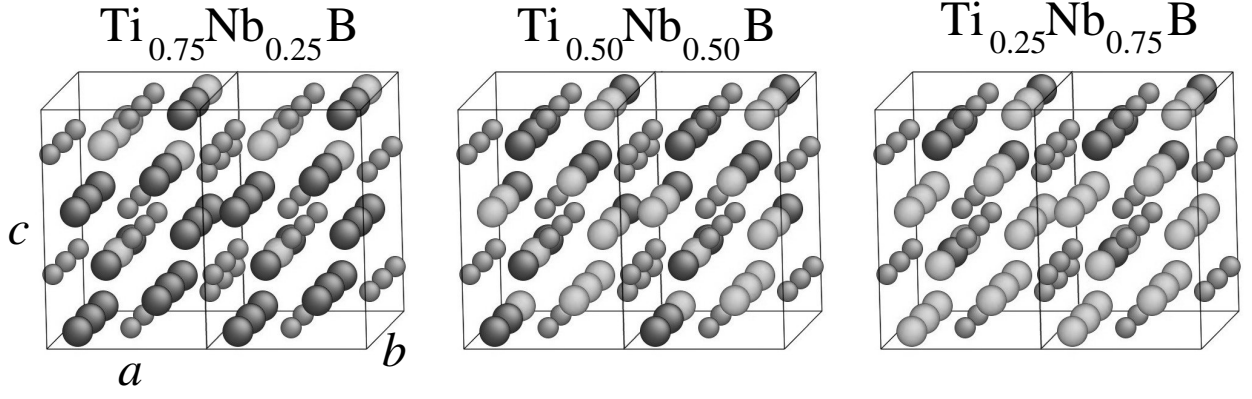


FIG. 1: Special quasirandom structures for $(\text{Ti}_{0.75}\text{Nb}_{0.25})\text{B}$, $(\text{Ti}_{0.5}\text{Nb}_{0.5})\text{B}$, and $(\text{Ti}_{0.25}\text{Nb}_{0.75})\text{B}$. The 48-atom supercell of Ti (large dark grey), Nb (large light grey), and B (small grey) is repeated in the a direction for visualization. The chemical identity in each periodic supercell is such that the neighbors for each atom approximates a truly random structure. These periodic supercell arrangements allow for efficient calculation of properties of a random alloy at the given compositions.

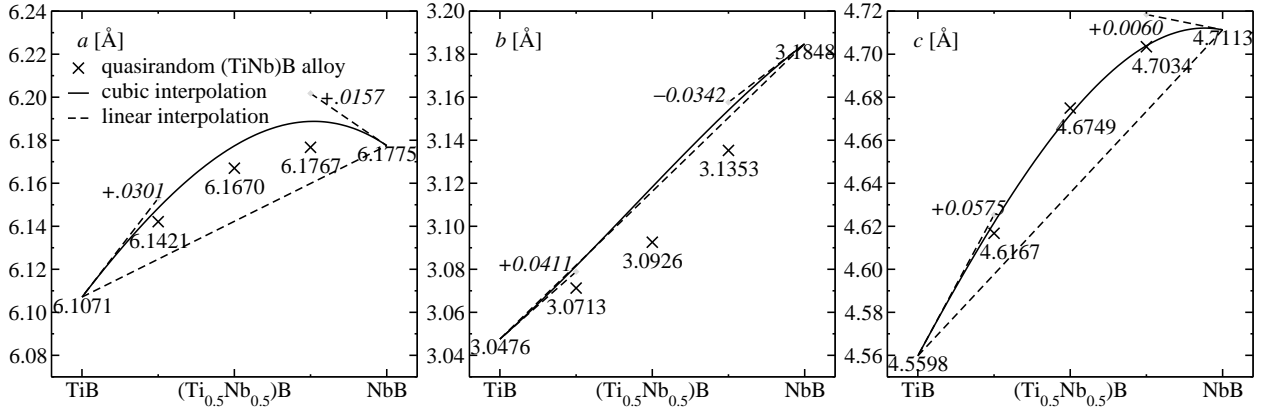


FIG. 2: Lattice constants for $(\text{Ti}_{1-x}\text{Nb}_x)\text{B}$ as a function of atomic concentration x of Nb. The values for pure TiB and NbB are shown as the endpoints of the interpolation curves. The solid line shows the cubic interpolation of Eqn. (3) for $\alpha = \beta = 0$; the straight dashed line indicates the result of a purely linear interpolation. The lattice misfits $y^{-1}dy(\text{TiB})/dc_{\text{Nb}}$ and $y^{-1}dy(\text{NbB})/dc_{\text{Ti}}$ are shown italicized with the corresponding slopes at the endpoints. For comparison, the lattice constants of the quasirandom (TiNb)B alloys are shown as single points for $x = 0.25, 0.50$, and 0.75 . The deviation from the predicted values and the quasirandom alloys are due to non-dilute concentrations reducing the strength of misfit.

from the TiB and NbB endpoints (Eqn. (3)), and compared with quasirandom (TiNb)B alloys. The results for pure TiB ($x = 0$) match previous calculations and experiments[5, 7]. The cubic interpolation of Eqn. (3) captures the effect of misfit for the small x and $(1 - x)$ limits. There was little difference in lattice and elastic constants and total energy between the quasirandom structures and the ordered structures, indicating that ordering will be weak, and has only a small effect on the properties of the borides. The quasirandom $(\text{Ti}_{0.5}\text{Nb}_{0.5})\text{B}$ alloy deviates from the prediction from misfits generally by reducing the effect of misfit, approaching the average of the TiB and NbB properties. In general, the cubic interpolation is not dramatically different from the linear interpolation, with the notable exception of C_{22} . In this case, the quasirandom alloys shows significant deviation in both b and C_{22} from the misfit prediction, especially for $(\text{Ti}_{0.5}\text{Nb}_{0.5})\text{B}$; these are expected to be related as decreasing lattice constants are connected to

increasing associated elastic constants. The large deviation indicates that experimental measurements of lattice constants and elastic for $(\text{Ti}_{1-x}\text{Nb}_x)\text{B}$ may provide potential insight into the effect of non-dilute concentrations on lattice and elastic properties.

Table II shows the Al and V lattice and elastic misfits in TiB and NbB. Generally, Al and V solutes decrease the lattice and elastic constants of TiB and NbB; the exception is V solutes in TiB, which have positive elastic misfits. The reduction of elastic constants contrasts the effects of Nb and Ti on TiB and NbB, which expand the lattice (c.f., Figure 2); this suggests that Al and V additions in the borides offer control of lattice matching by offsetting Ti and Nb expansion. The decrease in elastic response of TiB with Al and NbB with Al and V additions generally matches the Nb and Ti response, including the positive misfit for C_{22} ; this suggests less possible control over elastic response in the borides. While Al and

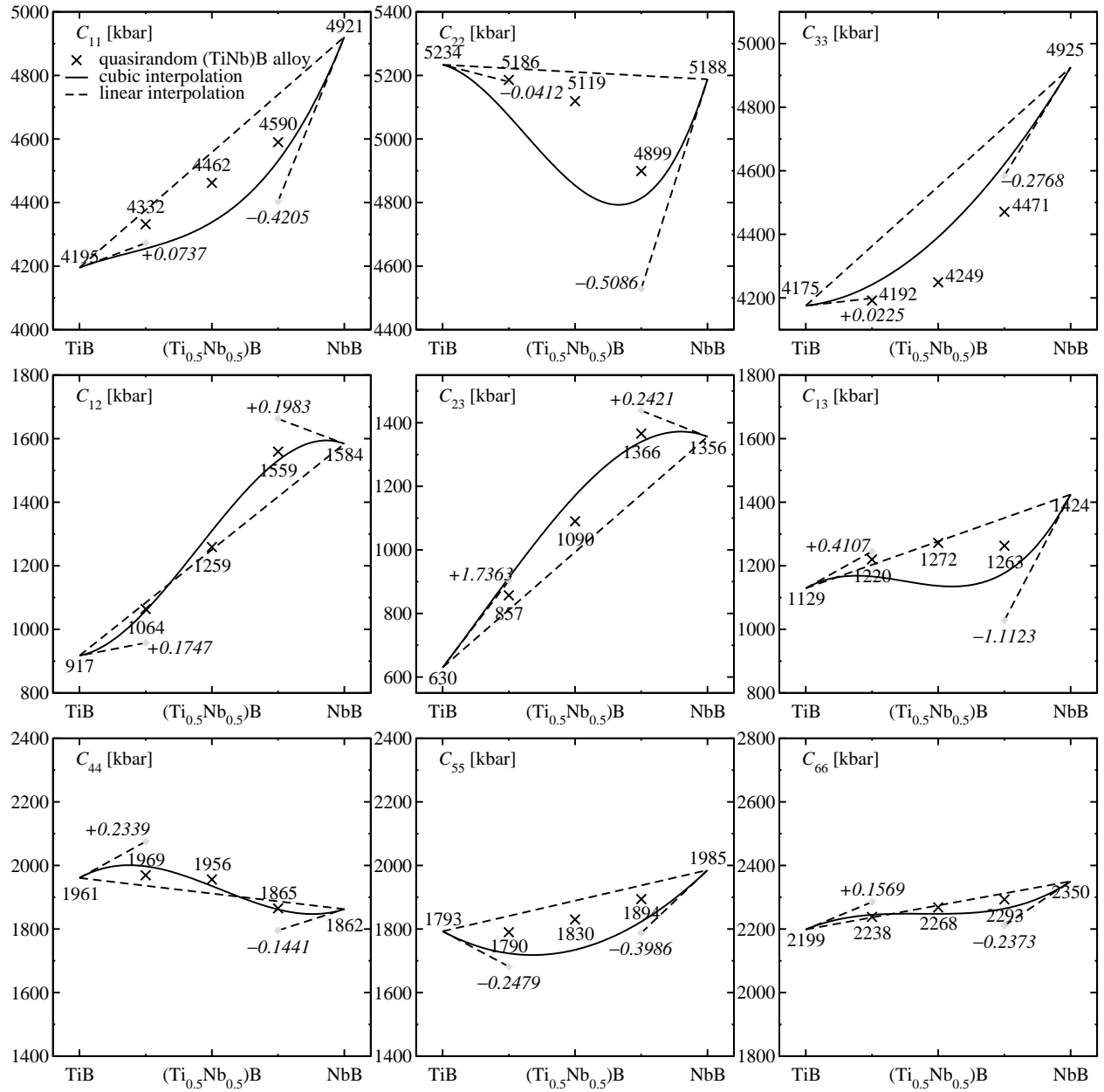


FIG. 3: Elastic constants for $(\text{Ti}_{1-x}\text{Nb}_x)\text{B}$ as a function of atomic concentration x of Nb. The values for pure TiB and NbB are shown as the endpoints of the interpolation curves. The solid line shows the cubic interpolation of Eqn. (3) for $\alpha = \beta = 0$; the straight dashed line indicates the result of a purely linear interpolation. The elastic misfits $y^{-1}dy(\text{TiB})/dc_{\text{Nb}}$ and $y^{-1}dy(\text{NbB})/dc_{\text{Ti}}$ are shown italicized with the corresponding slopes at the endpoints. For comparison, the elastic constants of the quasirandom (TiNb)B alloys are shown as single points for $x = 0.25, 0.50$, and 0.75 . The deviation from the predicted values and the quasirandom alloys are due to non-dilute concentrations reducing the strength of misfit. The general trend is a weakened elastic response in the random alloy compared with the linear interpolation of the endpoints.

V are present in many Ti alloys, the prediction of segregation to the borides with alloy chemistry and heat treatment is difficult; inferences from lattice constants are possible. For example, measurements of the lattice constants of the borides in Ti-6Al-4V (10 at.% Al, 4 at.% V) give $a = 6.11\text{\AA}$, $b = 3.05\text{\AA}$, $c = 4.56\text{\AA}$ [20]; assuming a sensitivity of $\pm 0.01\text{\AA}$, this predicts a maximum concentration of 8 at.% Al and 3 at.% V in the boride. Generally, experimental measurement of monoboride chemistry is crucial data for the prediction of boride

lattice and elastic constants in real alloys.

Table III contains the predicted lattice and elastic constants for monoborides in two different Ti alloys, using the monoboride chemistry from microprobe measurements[10]. The experimentally measured monoboride chemistry of the alloys both show nearly equal segregation of Ti and Nb to the borides, and appears to be nearly independent of the Nb concentration in the alloy. Al shows a small segregation to the boride, which validates the treatment of dilute Al in Eqn. (3).

TABLE III: Predicted single-crystal lattice and elastic constants for experimentally measured monoboride chemistries[10]. Microprobe analysis of monoborides in Ti-15Al-33Nb-5B (at.%) and Ti-22Al-26Nb-5B (at.%) alloys is used to interpolate lattice and elastic constants using Eqn. (3). As can be seen from Figure 3, the elastic constants near $x = 0.5$ are generally reduced below the average response of TiB and NbB.

Ti-15Al-33Nb-5B (at.%)				
chemistry [at.%]		lattice [Å] and elastic [kbar] constants		
Ti	22.32	$a = 6.1840$	$b = 3.1262$	$c = 4.6833$
Nb	29.50	$C_{11} = 4345$	$C_{22} = 4788$	$C_{33} = 4401$
Al	0.429	$C_{12} = 1376$	$C_{23} = 1237$	$C_{13} = 1133$
V	—	$C_{44} = 1906$	$C_{55} = 1726$	$C_{66} = 2227$
B	<i>balance</i>	<i>param: $x = 0.569$; $\alpha = 0.0082$; $\beta = 0$</i>		
Ti-22Al-26Nb-5B (at.%)				
chemistry [at.%]		lattice [Å] and elastic [kbar] constants		
Ti	22.23	$a = 6.1835$	$b = 3.1308$	$c = 4.6853$
Nb	31.46	$C_{11} = 4387$	$C_{22} = 4808$	$C_{33} = 4461$
Al	0.003	$C_{12} = 1396$	$C_{23} = 1242$	$C_{13} = 1136$
V	—	$C_{44} = 1907$	$C_{55} = 1756$	$C_{66} = 2249$
B	<i>balance</i>	<i>param: $x = 0.586$; $\alpha = 5.6 \times 10^{-5}$; $\beta = 0$</i>		

In both cases, the final B concentration is nearly 50 at.%; this is expected from the Ti-B phase diagram, which shows TiB to be a line compound with a homogeneity range of 49–50 at.% [7, 21, 22]. Microprobe measurements do not provide information regarding the possibility of local short-range Ti-Ti or Nb-Nb order in the boride. As Figure 2 shows, the lattice constants are expanded relative to the linear interpolation of TiB-NbB; Figure 3 also generally shows a reduction in elastic constants relative to the linear interpolation of TiB-NbB. Experimental verification of the predicted lattice and elastic constants can elucidate the effect of non-dilute concentrations in the boride lattice, through deviations from the random-alloy predictions.

Conclusion. The results illustrate the ability of electronic-structure calculations to predict lattice and elastic constants for real materials, especially in cases where experimental measurements are extremely difficult or time-consuming. The calculations for $(\text{Ti}_{1-x}\text{Nb}_x)\text{B}$ borides and the inclusion of dilute Al and V solutes provides a database for the prediction of lattice and elastic constants in real Ti alloys, which in turn can aid in the design of new materials. To model increasingly realistic material systems requires modern computational materials science techniques that investigate the changes in chemistry produced by solid solution, and the effect on material properties.

The author thanks D. Miracle, K. S. R. Chandran, and

C. Woodward for helpful discussions. The microprobe data was provided by C. Boehlert at Michigan State University. This research was performed while DRT held a National Research Council Research Associateship Award at AFRL. This research was supported in part by a grant of computer time from the DoD High Performance Computing Modernization Program at ASC/MSRC.

* Department of Material Science and Engineering, University of Illinois, Urbana-Champaign, 1304 W. Green Street, Urbana, IL 61801, USA; Electronic address: dtrinkle@uiuc.edu

- [1] T. M. T. Godfrey, P. S. Goodwin, and C. M. Ward-Close, *Adv. Eng. Mater.* **2**, 85 (2000).
- [2] R. Banerjee, P. C. Collins, and H. L. Fraser, *Adv. Eng. Mater.* **4**, 847 (2002).
- [3] S. Tamirisakandala, R. B. Bhat, J. S. Tiley, and D. B. Miracle, *J. Mater. Eng. Perform.* **14**, 741 (2005).
- [4] D. Hill, R. Banerjee, D. Huber, J. Tiley, and H. L. Fraser, *Scripta Mater.* **52**, 387 (2005).
- [5] K. B. Panda and K. S. R. Chandran, *Acta Mater.* **54**, 1641 (2006).
- [6] T. Hahn, ed., *International Tables for Crystallography*, vol. A (Dordrecht: Kluwer Academic, 1996), 4th ed.
- [7] B. F. Decker and R. Kasper, *Acta Crystall.* **7**, 77 (1954).
- [8] R. R. Atri, K. S. R. Chandran, and S. K. Jha, *Mater. Sci. Eng. A* **271**, 150 (1999).
- [9] S. Gorsse and D. B. Miracle, *Acta Mater.* **51**, 2427 (2003).
- [10] C. J. Cowen and C. J. Boehlert, *Mat. Sci. Forum* (2006), (submitted).
- [11] L. V. Artyukh, D. B. Borysov, A. A. Bondar, P. S. Martsenyuk, N. I. Tsygankenko, and T. Y. Velikanova, *High Temp. Mater. Process.* **25**, 75 (2006).
- [12] G. Kresse and J. Hafner, *Phys. Rev. B* **47**, RC558 (1993).
- [13] G. Kresse and J. Furthmüller, *Phys. Rev. B* **54**, 11169 (1996).
- [14] P. E. Blöchl, *Phys. Rev. B* **50**, 17953 (1994).
- [15] G. Kresse and D. Joubert, *Phys. Rev. B* **59**, 1758 (1999).
- [16] J. P. Perdew, in *Electronic Structure of Solids '91*, edited by P. Ziesche and H. Eschrig (Akademie Verlag, Berlin, 1991), pp. 11–20.
- [17] A. Zunger, S.-H. Wei, L. G. Ferreira, and J. E. Bernard, *Phys. Rev. Lett.* **65**, 353 (1990).
- [18] S.-H. Wei, L. G. Ferreira, J. E. Bernard, and A. Zunger, *Phys. Rev. B* **42**, 9622 (1990).
- [19] A. van de Walle, M. Asta, and G. Ceder, *CALPHAD* **26**, 539 (2002).
- [20] A. Genç, R. Banerjee, D. Hill, and H. L. Fraser, *Mat. Lett.* **60**, 859 (2006).
- [21] H. Baker, ed., *ASM handbook: Alloy phase diagrams*, vol. 3 (ASM International: Materials Park, OH, 1992).
- [22] X. Y. Ma, C. R. Li, Z. M. Du, and W. J. Zhang, *J. Alloy. Compd.* **370**, 149 (2004).